The Meteoritical Society

*Meteoritics & Planetary Science* 41, Nr 12, 1871–1881 (2006)
Abstract available online at http://meteoritics.org

# A study of Mg and K isotopes in Allende CAIs: Implications to the time scale for the multiple heating processes

Motoo ITO[1†], Hiroshi NAGASAWA[2], and Hisayoshi YURIMOTO[1††]

[1]Department of Earth and Planetary Sciences, Tokyo Institute of Technology, Ookayama, Meguro-ku, Tokyo 152-8551, Japan
[2]Department of Chemistry, Gakushuin University, Mejiro, Toshima-ku, Tokyo 171-8588, Japan
[†]Present address: NASA, Johnson Space Center, ARES Mail Code KR, 2101 NASA Parkway, Houston, Texas 77058, USA
[††]Present address: Division of Earth and Planetary Sciences, Hokkaido University, Sapporo 060-0810, Japan
[*]Corresponding author. E-mail: motoo.ito-1@nasa.gov

*(Received 09 November 2005; revision accepted 22 September 2006)*

**Abstract**–The measurements of magnesium and potassium isotopic compositions of refractory minerals in Allende calcium-aluminum-rich inclusions (CAIs), 7R-19-1, HN3-1, and EGG3 were taken by secondary ion mass spectrometry (SIMS). The 7R-19-1 contains $^{16}$O-rich and $^{16}$O-poor melilite grains and define a single isochron corresponding to an initial $^{26}$Al/$^{27}$Al ratio of $(6.6 \pm 1.3) \times 10^{-5}$. The Al-Mg isochron, O isotope measurements and petrography of melilite in 7R-19-1 indicate that $^{16}$O-poor melilite crystallized within 0.4 Myr after crystallization of $^{16}$O-rich melilite, suggesting that oxygen isotopic composition of the CAI-forming region changed from $^{16}$O-rich to $^{16}$O-poor within this time interval. The $^{16}$O-poor melilite is highly depleted in K compared to the adjacent $^{16}$O-rich melilite, indicating evaporation during remelting of 7R-19-1. We determined the isochron for $^{41}$Ca-$^{41}$K isotopic systematics in EGG3 pyroxene with $(4.1 \pm 2.0) \times 10^{-9}$ ($2\sigma$) as an initial ratio of $^{41}$Ca/$^{40}$Ca, which is at least two times smaller than the previous result (Sahijipal et al. 2000). The ratio of $^{41}$Ca/$^{40}$Ca in the EGG3 pyroxene grain agrees within error with the value obtained by Hutcheon et al. (1984). No evidence for the presence of $^{41}$K excess (decay product of a short-lived radionuclide $^{41}$Ca) was found in 7R-19-1 and HN3-1. We infer that the CAI had at least an order of magnitude lower than canonical $^{41}$Ca/$^{40}$Ca ratio at the time of the CAI formation.

## INTRODUCTION

Calcium-aluminum-rich inclusions (CAIs) in the Allende CV3 meteorite have experienced several successive stages of melting based on the micro-analysis of inter- and intramineral distributions of O isotopes in the Allende CAI, 7R-19-1 (Yurimoto et al. 1998; Ito et al. 2004). The determination of the time interval between each melting stage is important in understanding the CAI-forming environment and history in the very early solar system. In order to estimate time intervals of multiple CAI-heating phenomena, the distributions of the short-lived nuclides $^{26}$Al and $^{41}$Ca with different half-lives in a CAI may serve as a useful measure.

$^{26}$Al is a short-lived radionuclide with a half-life of 0.72 Myr and its presence in the early solar system is conclusively established (e.g., MacPherson et al. 1995). This half-life enables a time resolution of less than 1 Myr (e.g., Bizzarro et al. 2004). The high resolution is necessary to evaluate the time interval of the events that produced the complicated structure of CAIs. Even higher temporal resolution is possible by exploiting the $^{41}$Ca-$^{41}$K system since the $^{41}$Ca half-life (0.1 Myr) is much smaller than that of $^{26}$Al. Several CAI minerals, such as melilite, fassaite, hibonite, and perovskite, are good targets for these measurements owing to their high Ca/K ratios. Differences of isochrons within 1 Myr are easily determined by $^{41}$Ca-$^{41}$K isotopic systematics.

The existence of $^{41}$Ca in the early solar system was first reported by Hutcheon et al. (1984). The initial $^{41}$Ca/$^{40}$Ca value was assumed to be $(8 \pm 3) \times 10^{-9}$ from pyroxenes in two Allende CAIs. Later, Srinivasan et al. (1994, 1996) reported the presence of $^{41}$K excess ($^{41}$K$^{*}$) corresponding to the initial $^{41}$Ca/$^{40}$Ca ratio of $(1.41 \pm 0.14) \times 10^{-8}$ in several CAIs from Efremovka. These results have been confirmed by K isotope measurements of the same CAIs by Ireland et al. (1999) who reported the initial $^{41}$Ca$^{40}$Ca ratio of $(1.7 \pm 0.2) \times 10^{-8}$. Sahijpal et al. (2000) measured hibonite from the Murchison CM meteorite with an initial $^{41}$Ca/$^{40}$Ca value of $(1.10 \pm 0.34) \times 10^{-8}$, and hibonite with an initial $^{41}$Ca/$^{40}$Ca value of $(1.35 \pm 0.55) \times 10^{-8}$ from the Allende CV3 meteorite, and EGG3 pyroxene with an initial $^{41}$Ca/$^{40}$Ca value of $(1.17 \pm 0.24) \times$

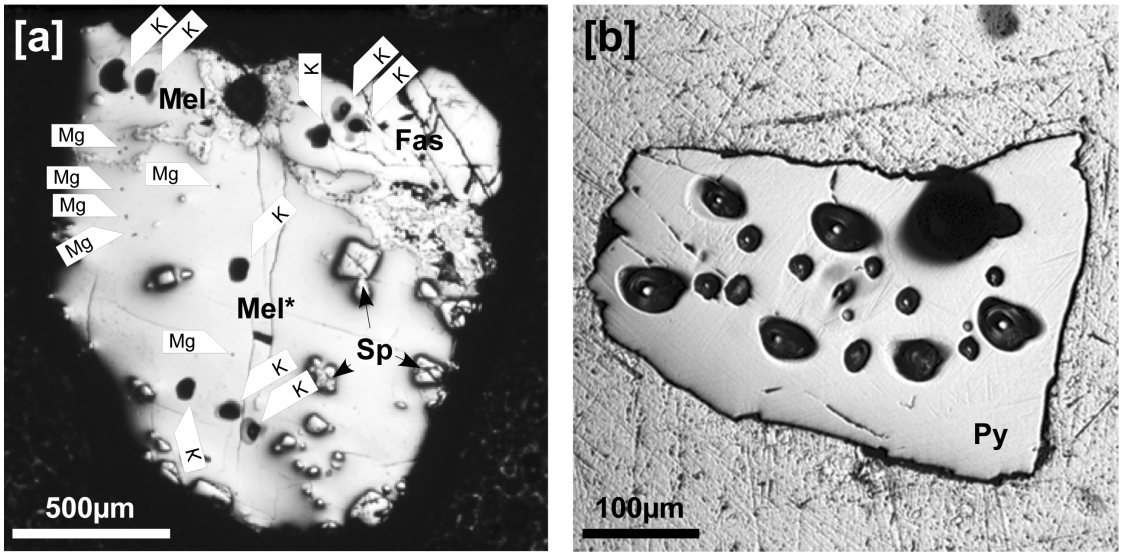


Fig. 1. Photomicrographs of 7R-19-1(a) and EGG3 pyroxene after the K and Mg isotopic measurements with SIMS. a) 7R-19-1(a). Large pits are K isotopic measurement. Abbreviations: Mel = $^{16}$O-poor melilite, Mel* = $^{16}$O-rich melilite, Fas = fassaite, Sp = spinel. Large (~15 μm in diameter surrounding relatively large halo because of the tailing of O primary ion beam) and small (~3 μm in diameter) pits represent K and Mg isotopic measurements with SIMS, respectively. b) EGG3 pyroxene. Craters are for K isotopic measurements with SIMS.

$10^{-8}$ from Allende; some of the Murchison hibonites were devoid of both $^{26}$Mg excess ($^{26}$Mg$^*$) and $^{41}$K$^*$. Ushikubo et al. (2000) measured a FUN-like hibonite inclusion in the Kainsaz CO3 meteorite. The inclusion obtained an initial $^{26}$Al/$^{27}$Al value of $(5.3 \pm 0.3) \times 10^{-5}$ and an initial $^{41}$Ca/$^{40}$Ca value of $(1.1 \pm 0.6) \times 10^{-8}$. The initial $^{41}$Ca abundance for the solar system appears uncertain by at least a factor of two until now.

According to the previous studies (Srinivasan et al. 1996; Ushikubo et al. 2000; Sahijpal et al. 1998, 2000), a CAI with a $^{41}$K$^*$ always has $^{26}$Mg$^*$. However, Srinivasan and Bischoff (2001) reported that a CAI with $^{41}$K$^*$ from CH chondrite has no initial $^{26}$Al. This lack of correlation between $^{26}$Al and $^{41}$Ca suggested that the source for $^{26}$Al and $^{41}$Ca may not be necessarily the same as suggested earlier by Sahijpal et al. (1998).

In this study, we have confirmed $^{41}$K$^*$ from $^{41}$Ca decay in EGG3 pyroxene having known a $^{41}$K$^*$ under our measurement setting, and also analyzed distributions of both radiogenic $^{26}$Mg$^*$ and $^{41}$K$^*$ in two Allende CAIs, 7R-19-1 and HN3-1, in which the O isotopic distributions were well established (Mayeda et al. 1986; Yurimoto et al. 1994, 1998; Ito 1999; Ito et al. 2004). The K isotopic compositions were measured following the completions of the Mg isotopic measurement at the same spot of CAI constituent minerals.

## EXPERIMENTAL PROCEDURE

### Meteorite Samples and Terrestrial Standards

The Allende CAIs used in this study are HN3-1, 7R-19-1, and EGG3 pyroxene. Figure 1 shows photomicrographs of 7R-19-1(a) and EGG3 pyroxene after the Mg and K isotopic measurement by SIMS.

HN3-1 is a typical coarse-grained type B1 CAI. HN3-1 is large (~1 cm) and consists of melilite mantle ($Åk_{30–60}$), small spinel grains, anorthite, and fassaite (Nagahara et al. 1987). The bulk chemical composition of HN3-1 and oxygen isotopic compositions of its minerals are summarized in Table 1. The O isotopic characteristics show typical O isotope ratios for CV CAI melilite ($\delta^{17,18}$O ~ 0‰), and spinel ($\delta^{17,18}$O ~ –40‰) crystals (Mayeda et al. 1986; Yurimoto et al. 1994; Ito 1999). Koike et al. (1994) reported that the initial $^{26}$Al/$^{27}$Al ratio for HN3-1 have variations of $(3–5) \times 10^{-5}$.

7R-19-1 is a fassaite-rich, compact type A CAI. 7R-19-1 consists mainly of melilite ($Åk_{23–26}$, 60–70 vol%), fassaite (~10 vol%), and spinel grains (~10 vol%). Hibonites, perovskites, and anorthites occur in the CAI as minor minerals. This CAI has been well documented for its petrographic texture, chemical compositions, and O isotopic characteristics (Yurimoto et al. 1998; Ito et al. 2004). Epoxy-mounted samples of 7R-19-1(a) and (d) were used in this study.

An EGG3 pyroxene grain from Caltech collection was provided by Dr. Goswami. The petrographic texture, chemical composition, and isotopic characteristics of EGG3 were published by Meeker et al. (1983), Hutcheon et al. (1984), and Sahijpal et al. (2000). EGG3 is a type B CAI. It is a subspherical coarse-grained inclusion, composed primarily of Ti-rich fassaite, anorthite, spinel, and melilite (Meeker et al. 1983). The initial $^{41}$Ca/$^{40}$Ca ratios inferred for the EGG3 pyroxenes are $(8 \pm 3) \times 10^{-9}$ and $(1.17 \pm 0.24) \times 10^{-8}$ by Hutcheon et al. (1984) and Sahijpal et al. (2000), respectively. There are no differences between these values if taking account

of errors. EGG3 pyroxene was analyzed to ensure that Ca-K isotopic systematics in meteoritic phases can be analyzed meaningfully using TiTech ims-1270 SIMS instrument.

For K isotopic microanalysis by SIMS, several terrestrial standards were measured to establish the reproducibility of the reference K isotopic compositions with wide variations of $10^3$ to $10^6$ in $^{40}Ca/^{39}K$ ratio. The standards are NIST SRM 613, 615, 617, and anorthite from Miyakejima, Japan, augite from Takashima, Japan, synthetic gehlenite, åkermanite and CAI-Px-2 pyroxene glass that was prepared at Caltech with high Ca/K ratio (Table 2).

**Magnesium Isotope Analysis**

The epoxy-mounted samples were coated with a 30 nm Au thin film to eliminate the electrostatic charge on the sample surface. Mg isotopic measurements of 7R-19-1(a) and (d) were carried out by the TiTech ims-1270 SIMS instrument. The typical $^{16}O^-$ primary ion beam size was 2–3 μm in diameter. A mass resolution was set to 4000, sufficient to remove hydride interference $[^{24}MgH]^+$ on $[^{25}Mg]^+$. The isotopic measurements were made in the peak-jumping mode through the mass sequence $^{24}Mg$, $^{25}Mg$, $^{26}Mg$, and $^{27}Al$. Each analysis consisted of 10 blocks of 10 cycles of counting $[^{24}Mg]^+$ for 2 s, $[^{25}Mg]^+$ for 6 s, $[^{26}Mg]^+$ for 6 s, and $[^{27}Al]^+$ for 2 s, which took about 35 min. The other conditions of Mg isotopic measurement are similar to those in Koike et al. (1994) and Maruyama and Yurimoto (2003).

**Potassium Isotope Analysis**

The K isotopic compositions were analyzed following the completions of the Mg isotopic studies at the same spot. Because of the importance of avoiding any K contamination (S. Sahijipal, personal communication), we did not perform any further treatments to the sample prior to the $^{41}Ca$-$^{41}K$ isotopic analysis. The sample integrity was also protected by heating in ultrapure water prior to Au coating.

We used the TiTech ims-1270 for analyzing of $^{41}Ca$-$^{41}K$ isotopic systematics. High transmission is necessary to achieve the high-precision measurement for K isotope analysis because of the extremely low $^{41}K^*$ count rate. The ims-1270 SIMS instrument can be operated in two different modes of the secondary ion optics, circular and XY. The circular mode is commonly used in all the CAMECA SIMS series. The XY mode uses a pair of rectangular lenses settled in front of the entrance of the magnetic sector in addition to the setting of the circular mode. The XY mode was developed for the purpose of achieving the combination of high ion transmission and high mass resolution compared with circular mode on the ims-1270 SIMS instrument (De Chambost et al. 1997). The XY mode offers an increase in secondary ion transmission of a factor of two to four times higher than that of circular mode (De Chambost et al. 1997). We used both of these modes for the K isotopic measurements, and we compare the results below. The analytical conditions for the circular and XY modes were identical.

Table 1. Previous studies of HN3-1.

| Bulk chemical compositions (wt%)[a] | | O isotopes (‰) | | Mg isotopes[b] |
|---|---|---|---|---|
| MgO | 9.3 | $\delta^{17}O_{SMOW}$ | $\delta^{18}O_{SMOW}$ | $(^{26}Al/^{27}Al)_0$ |
| $Al_2O_3$ | 29.2 | Melilite | | $3.12 \times 10^{-5}$ |
| $SiO_2$ | 30.9 | 1.2 | 7.8[c] | |
| CaO | 27.4 | –4.31 | –0.45[d] | $^{26}Mg$ (‰) |
| $TiO_2$ | 1.2 | Spinel | | 3.37 |
| FeO | 0.8 | –36.4 | –37.9[c] | |
| $Na_2O$ | 0.2 | –42.79 | –40.47[d] | |
| S | 0.0 | n.a.[e] | –38[f] | |
| Total | 98.2 | | | |

[a]Nagahara et al. (1987).
[b]Koike et al. (1993).
[c]Ito (1999).
[d]Mayeda et al. (1986).
[e]n.a.: no analysis.
[f]Yurimoto et al. (1994).

A focused $^{16}O^-$ primary ion beam accelerated with 23 keV was used and the beam spot size was 12–15 μm in diameter. A mass resolving power was set to 5500, sufficient to resolve the main hydride interference of $[^{40}CaH]^+$ on $[^{41}K]^+$. The positive secondary ions of the following masses, $[^{39}K]^+$, 40.7, $[^{41}K]^+$, $[^{40}CaH]^+$, $[^{40}Ca^{43}Ca]^{++}$, $[^{42}Ca]_{tail}^+$, $[^{42}Ca]^+$, and $[^{43}Ca]^+$ were detected by an electron multiplier using a pulse counting mode. The background of counting system was determined by monitoring mass 40.7 during the measurement. Each analysis consisted of 10 blocks of 6 cycles of counting $[^{39}K]^+$ for 10 s, 40.7 for 40 s, $[^{41}K]^+$ for 40 s, $[^{40}CaH]^+$ for 1 s, $[^{40}Ca^{43}Ca]^{++}$ for 40 s, $[^{42}Ca]_{tail}^+$ for 10 s, $[^{42}Ca]^+$ for 1 s, and $[^{43}Ca]^+$ for 1 s, giving a total analysis time of about 90 min.

Analytical masses and the calculation of "true radiogenic $^{41}K$" intensity were similar to those described in Srinivasan et al. (1996). The interference for the mass $^{41}K$ peak are combinations of the $[^{40}Ca^{42}Ca]^{++}$, the $[^{40}CaH]_{tail}^+$, and the background noise of the instrument. The background noise slightly varies under different instrumental conditions of the detection system. We carefully determined that the noise was 0.02–0.08 cps except EGG3 measurements. The noise for the EGG3 measurement was 0.02–0.58 cps. The relatively high background was due to exchange of the EM. The most critical interference is $[^{40}Ca^{42}Ca]^{++}$ peak on the $^{41}K^+$ (Hutcheon et al. 1984). However, the $[^{40}Ca^{42}Ca]^{++}$ peak is not possible to separate from $^{41}K^+$ peak at mass resolving power of 5500. We followed the approach of Hutcheon et al. (1984), which is discussed in detail by Srinivasan et al. (1996), for the interference correction of $[^{40}Ca^{42}Ca]^{++}$ at $^{41}K^+$ and assuming as follows:

$$\frac{[^{40}Ca^{43}Ca]^{++}}{[^{43}Ca]^{+}} = \frac{[^{40}Ca^{42}Ca]^{++}}{[^{42}Ca]^{+}} \quad (1)$$

Table 2. K isotopic data of terrestrial standards.[a]

| Standard | | N[b] | $^{40}Ca/^{39}K$ (2σ)[c] | $^{41}K/^{39}K$ (2σ) |
|---|---|---|---|---|
| NIST[d] | SRM613 | 2 | $(1.38 \pm 0.07) \times 10^3$ | 0.0717 ± 0.0010 |
| | SRM615 | 5 | $(2.68 \pm 0.25) \times 10^3$ | 0.0718 ± 0.0008 |
| | SRM617 | 1 | $(3.01 \pm 0.07) \times 10^3$ | 0.0721 ± 0.0002 |
| Miyakejima anorthite | | 3 | $(4.69 \pm 0.16) \times 10^3$ | 0.0722 ± 0.0001 |
| Takashima augite | | 3 | $(1.97 \pm 0.11) \times 10^4$ | 0.0721 ± 0.0006 |
| CAI-Px-2[e] | | 2 | $(3.00 \pm 0.14) \times 10^6$ | 0.0735 ± 0.0051 |
| Synthetic åkermanite[f] | | 4 | $(1.18 \pm 0.19) \times 10^5$ | 0.0722 ± 0.0023 |
| Synthetic gehlenite[f] | | 12 | $(3.52 \pm 2.24) \times 10^6$ | 0.0641 ± 0.0089 |
| All terrestrial standards | | | Initial $^{40}Ca/^{39}K$ (2σ) $(-0.4 \pm 1.4) \times 10^{-9}$ | $^{41}K/^{39}K$-intercept (2σ) 0.0722 ± 0.0001 |

[a]All data were obtained by circular mode.
[b]Number of analyses.
[c]Errors were calculated from the error propagation based on multiple measurements. The error of SRM 617 was calculated from the counting statistics of the measurement.
[d]NIST SRM series standards were used for calculation of $^{40}Ca/^{39}K$ ratio in minerals of CAIs.
[e]Sample prepared at Caltech (Provided by Dr. Goswami).
[f]The $^{40}Ca/^{39}K$ ratios for åkermanite and gehlenite were calculated from NIST SRM standards.

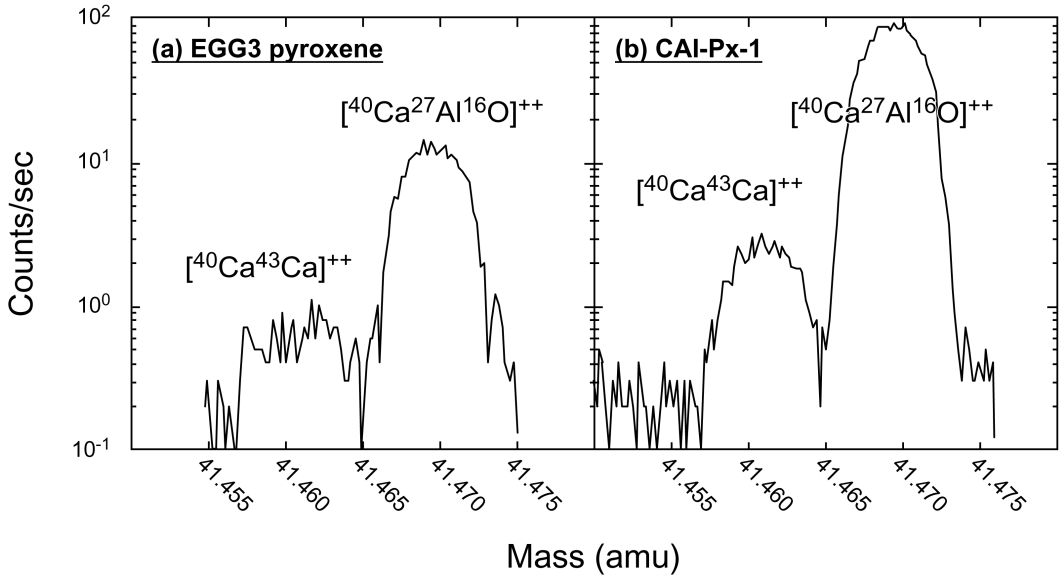


Fig. 2. High mass resolution (M/ΔM ~5500) spectra at mass 41.5 for (a) Allende CAI EGG3 pyroxene and (b) synthetic CAI-Px-1 (provided by Dr. Goswami and made by Dr. Hutcheon). The mass of $[^{40}Ca^{43}Ca]^{++}$ and $[^{40}Ca^{27}Al^{16}O]^{++}$ are 41.4607 and 41.4695, respectively.

The $[^{40}Ca^{43}Ca]^{++}$ signal monitored at mass ~41.5 was typically less than 1 cps under measurement conditions. To determine the $[^{40}Ca^{43}Ca]^{++}$ peak position in terrestrial and meteoritic minerals, we have carefully monitored the $[^{40}Ca^{27}Al^{16}O]^{++}$ peak during the measurement. Figure 2 shows the typical high mass resolution spectrum for EGG3 pyroxene and CAI-Px-2. The $[^{40}Ca^{27}Al^{16}O]^{++}$ peak (m/e= 41.4695) was separated from the $[^{40}Ca^{43}Ca]^{++}$ peak (m/e= 41.4607) by 0.0088 amu (Fig. 2). We obtained the value of $[^{40}Ca^{43}Ca]^{++}/[^{43}Ca]^{+}$ ratio for every measurement cycle.

In order to ensure accurate measurements of K isotope ratio of meteoritic minerals with high $^{40}Ca/^{39}K$ ratio (>$10^5$), we have analyzed several terrestrial minerals with wide variations (103-106) as a standard (Table 2; Fig. 3). NIST SRM613, 615, and 617 were used for the calculation of $^{40}Ca/^{39}K$ ratio of measured meteoritic mineral phases. Then, we have confirmed $^{41}K/^{39}K$ and $^{40}Ca/^{39}K$ ratios in Miyakejima anorthite, Takashima augite and CAI-Px-2, which is provided by Dr. Goswami and prepared at Caltech by Dr. Hutcheon having known K concentration. Finally, we have measured $^{41}K/^{39}K$ and $^{40}Ca/^{39}K$ ratios in synthetic åkermanite and gehlenite. This routine procedure of standards measurements allowed us to provide accurate K isotope ratios in meteoritic mineral phases with high $^{40}Ca/^{39}K$ ratio.

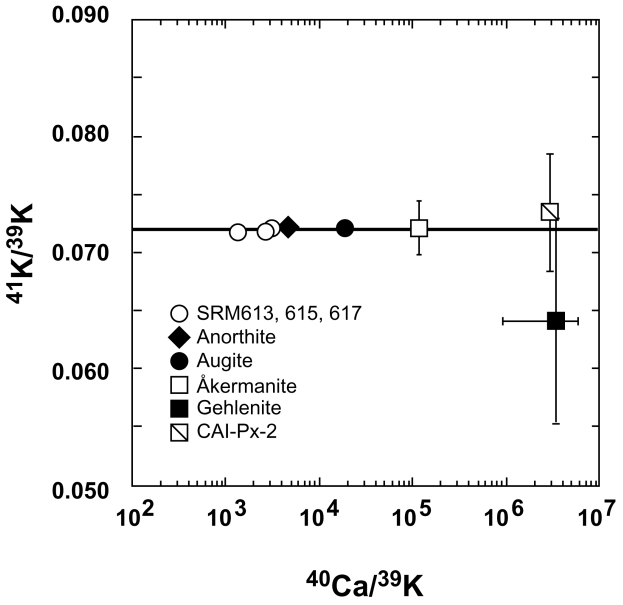


Fig. 3. Measured K isotopic compositions in five terrestrial standards of anorthite from Miyakejima, Japan, augite from Takashima, Japan, synthetic åkermanite, synthetic gehlenite, synthetic CAI-Px-2 standard, and NIST SRM 613, 615, 617 glasses with wide variation of Ca/K ratios among four orders of magnitude. The solid line represents the terrestrial K isotopic ratios ($^{41}K/^{39}K$ = 0.072, Garner et al. 1975). Error bars are ±2σ.

Table 3. Al-Mg isotopic data in melilite, hibonite, and fassaite from Allende CAI 7R-19-1.

| Phase | | $^{27}Al/^{24}Mg$ (2σ) | $\delta^{26}Mg$ (‰)[a] ($2\sigma_{mean}$) | |
|---|---|---|---|---|
| 7R-19-1(a) | | | | |
| Melilite | Ma#01 | 15.2 ± 0.2 | 7.8 ± 3.2 | Mel*[b] |
| | Ma#02 | 10.5 ± 0.4 | 3.5 ± 3.0 | Mel[c] |
| | Ma#03 | 14.6 ± 0.5 | 5.6 ± 3.0 | Mel* |
| | Ma#04 | 12.9 ± 0.2 | 5.3 ± 2.5 | Mel* |
| | Ma#05 | 8.8 ± 0.1 | 4.9 ± 2.4 | Mel |
| | Ma#06 | 9.6 ± 0.1 | 4.9 ± 2.8 | OG[d] |
| | Ma#07 | 12.5 ± 0.1 | 4.8 ± 2.9 | Mel* |
| | Ma#08 | 8.3 ± 0.1 | 3.4 ± 2.3 | OG |
| Fassaite | Fa#01 | 2.1 ± 0.1 | 0.9 ± 1.3 | [e] |
| 7R-19-1(d) | | | | |
| Melilite | Md#01 | 21.0 ± 1.0 | 6.9 ± 3.9 | $^{16}$O-poor |
| | Md#02 | 2.3 ± 0.1 | 0.2 ± 1.3 | $^{16}$O-poor |
| | Md#03 | 10.8 ± 0.6 | 6.0 ± 2.6 | $^{16}$O-poor |
| Hibonite | Hd#01 | 19.7 ± 0.7 | 8.2 ± 3.9 | $^{16}$O-rich |
| | Hd#02 | 18.0 ± 0.5 | 10.6 ± 3.3 | $^{16}$O-rich |

[a]$(^{25}Mg/^{24}Mg)_{REF}$ and $(^{26}Mg/^{24}Mg)_{REF}$ are assumed to 0.12663 and 0.13932, respectively. (Catanzaro et al. 1966).
[b]Mel*: $^{16}$O-poor melilite.
[c]Mel: $^{16}$O-rich melilite.
[d]OG: $^{16}$O-poor overgrown melilite on Mel* adjacent to Mel.
[e]$\delta^{17,18}O_{SMOW}$ in fassaite ranges from –20 to 0‰.

## RESULTS

### Magnesium Isotope Measurements

The results obtained for the Mg isotopic measurements of melilite, fassaite, and hibonite from the Allende CAIs 7R-19-1(a) and (d) are given in Table 3. These data show the presence of live $^{26}$Al in the CAIs at the time of their crystallization. The 7R-19-1(a) CAI contains two grains of $^{16}$O-poor melilite and $^{16}$O-rich melilite. The $^{16}$O-rich melilite is overgrown by $^{16}$O-poor melilite (Yurimoto et al. 1998). Mg isotopic compositions were measured from points in the $^{16}$O-rich, the $^{16}$O-poor, and the overgrown melilite as well as in fassaite in 7R-19-1(a). All data define a single isochron with $(^{26}Al/^{27}Al)_0$ of $(6.6 \pm 1.3) \times 10^{-5}$ (2σ) and initial $\delta^{26}Mg$ is (–0.4 ± 0.9)‰ (2σ) (Fig. 4).

### Potassium Isotope Measurements

In order to correct the measured $^{41}$K signal for the unresolved $[^{40}Ca^{42}Ca]^{++}$ interference, we used the $[^{40}Ca^{43}Ca]^{++}/[^{43}Ca]^{+}$ values determined in each meteoritic phase following procedures described above. In Table 4, we show the values of $[^{40}Ca^{43}Ca]^{++}/[^{43}Ca]^{+}$ of meteoritic phases in different CAIs together with the values of terrestrial analog. The $[^{40}Ca^{43}Ca]^{++}/[^{43}Ca]^{+}$ values of melilite in HN3-1 and 7R-19-1, synthetic åkermanite, and gehlenite ranged from 1.1–1.2 × $10^{-5}$. It seems that the $[^{40}Ca^{43}Ca]^{++}/[^{43}Ca]^{+}$ value depends on the composition of the melilite solid solution. The $[^{40}Ca^{43}Ca]^{++}/[^{43}Ca]^{+}$ values of meteoritic fassaite in EGG3, HN3-1, and 7R-19-1 were similar to each other at ~2 × $10^{-5}$. The values of terrestrial pyroxenes of CAI-Px-2 and Takashima augite were slightly smaller than those of meteoritic pyroxene (Table 4). The $[^{40}Ca^{43}Ca]^{++}/[^{43}Ca]^{+}$ values of terrestrial anorthite, meteoritic phases of hibonite, anorthite, and perovskite were very close to each other of ~1.0–1.1 × $10^{-5}$ (Table 4). The $[^{40}Ca^{43}Ca]^{++}/[^{43}Ca]^{+}$ values measured by the circular and XY modes for each phases are the same within error.

The observed $^{41}K/^{39}K$ ratios in all terrestrial standards (NIST SRM 613, 615, 617, anorthite from Miyakejima, Japan, augite from Takashima, Japan, synthetic gehlenite and åkermanite, and CAI-Px-2) are close to the recommended value of 0.072 (Garner et al. 1975) within the limits of our experimental uncertainties (Table 2; Fig. 3). In order to detect an initial $^{41}Ca/^{40}Ca$ of ~$10^{-8}$ from meteoritic phases, the Ca/K ratios should be greater than $10^5$. We have prepared two terrestrial samples of gehlenite and CAI-Px-2 having Ca/K > $10^6$ (Table 2 and Fig. 3). The data of CAI-Px-2 with Ca/K = 3 × $10^6$ was good agreement with the normal $^{41}K/^{39}K$ ratio. On the other hand, the data of synthetic gehlenite with Ca/K = 3.5 × $10^6$ was 0.0641 ± 0.0089 (2σ). It may seem to be lower than the average of terrestrial standards although the data overlapped the normal ratio of 0.072 at the 2σ limit (Table 2; Fig. 3). The low $^{41}K/^{39}K$ ratio may be explained by an overcorrection for mass 41 peak because there are possible

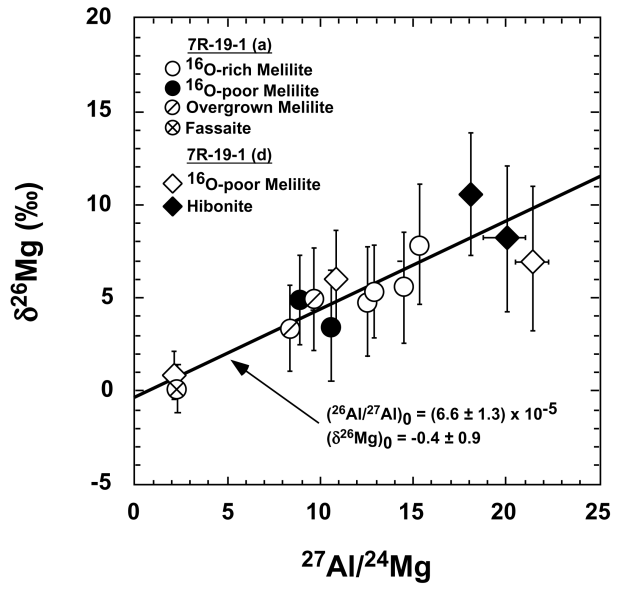


Fig. 4. Mg isotopic compositions in melilite, fassaite, and hibonite in 7R-19-1 Allende CAI. The solid lines represent the evolution diagram of $^{26}$Al-$^{26}$Mg isotopic systematics with the initial $^{26}$Al/$^{27}$Al of $(6.6 \pm 1.3) \times 10^{-5}$ (2σ) for 7R-19-1. The uncertainty in the slope of the best fit is ±2σ. Intercept defined as $\delta^{26}$Mg are (–0.4 ± 0.9)‰ (2σ). Error bars for the individual measured point for $^{27}$Al/$^{24}$Mg and $\delta^{26}$Mg are ±2σ and ±2$\sigma_m$, respectively.

scattered ions in the background measurement at mass 40.7. A correlation line fitted to all of the terrestrial data has a slope corresponding to $(^{41}Ca/^{40}Ca)_0 = (-0.4 \pm 1.4) \times 10^{-9}$ (2σ) and an intercept of $^{41}K/^{39}K = 0.0722 \pm 0.0001$ (2σ) (Table 2). Based on the terrestrial standards data, a detection limit of ~$10^{-9}$ can be inferred for the $(^{41}Ca/^{40}Ca)_0$.

Data of EGG3 pyroxene for $^{41}$Ca-$^{41}$K isotopic systematics are given in Table 5. We have used both circular and XY modes for this measurement at the same measured spot in order to confirm that there are no systematic changes of the isotopic ratio by the two different ion optic settings of mass spectrometer. The isochron for $^{41}$Ca-$^{41}$K isotopic systematics in EGG3 pyroxene measured by both circular and XY mode is $(4.1 \pm 2.0) \times 10^{-9}$ (2σ) (Table 5; Fig. 5). Hutcheon et al. (1984) and Sahijipal et al. (2000) reported that EGG3 pyroxene has different isochrons of $(^{41}Ca/^{40}Ca)_0 = (8 \pm 3) \times 10^{-9}$ and $(1.17 \pm 0.24) \times 10^{-8}$, respectively (Fig. 5). The value in this study is about two times smaller than the previous results. The intercept of $^{41}K/^{39}K$ for EGG3 pyroxene in this study of 0.0659 ± 0.0042 (2σ) (Table 5).

The data of $^{41}$Ca-$^{41}$K isotopic systematics for melilite, fassaite, hibonite, and perovskite in 7R-19-1 and for melilite, anorthite, and fassaite in HN3-1 CAIs from Allende meteorite analyzed in this study are given in Table 6. Several measured spots of K isotopes were the same positions of Mg isotopic analyses, as indicated in Table 6. The $^{41}K/^{39}K$ ratios of the CAI minerals are similar to the terrestrial value at $Ca/K < 10^5$, then gradually decrease with $Ca/K > 10^5$ reaching a minimum

Table 4. The values of $(^{40}Ca^{43}Ca)^{++}/(^{40}Ca)+$ of terrestrial standards and meteoritic phases.

| Standard | | N[a] | $(^{40}Ca^{43}Ca)^{++}/(^{40}Ca)^{+}$ (2σ)[b] |
|---|---|---|---|
| Terrestrial standard | | | |
| Miyakejima anorthite | | 3 | $(1.00 \pm 0.14) \times 10^{-5}$ |
| Takashima augite | | 3 | $(1.66 \pm 0.09) \times 10^{-5}$ |
| CAI-Px-2[c] | | 2 | $(1.88 \pm 0.01) \times 10^{-5}$ |
| Synthetic åkermanite | | 4 | $(1.23 \pm 0.13) \times 10^{-5}$ |
| Synthetic gehlenite | | 12 | $(1.08 \pm 0.26) \times 10^{-5}$ |
| Meteoritic phases | | | |
| Melilite | HN3-1 | 7 | $(1.22 \pm 0.26) \times 10^{-5}$ |
| | 7R-19-1 | 10 | $(1.13 \pm 0.27) \times 10^{-5}$ |
| Fassaite | HN3-1 | 3 | $(2.04 \pm 0.08) \times 10^{-5}$ |
| | 7R-19-1 | 4 | $(2.19 \pm 0.26) \times 10^{-5}$ |
| | EGG3 | 9 | $(2.15 \pm 0.62) \times 10^{-5}$ |
| Hibonite | 7R-19-1 | 2 | $(1.04 \pm 0.01) \times 10^{-5}$ |
| Anorthite | HN3-1 | 3 | $(1.09 \pm 0.13) \times 10^{-5}$ |
| Perovskite | 7R-19-1 | 1 | $1.09 \times 10^{-5}$ |

[a]Number of analyses.
[b]Errors were calculated from the multiple measurements.
[c]Sample prepared at Caltech (Provided by Dr. Goswami).

between $10^6 < Ca/K < 10^7$ and then increases again but rarely goes above the terrestrial value (0.072). This may reflect some analytical uncertainty or a problem with Ca-K isotope systematics in melilite as the data for high Ca/K ($>2 \times 10^5$) are primarily for melilite, with a couple of exceptions. Srinivasan et al. (1996) noted that the Ca-K systematics may not be well behaved in melilite. These smaller $^{41}K/^{39}K$ ratios, around Ca/K ~$10^6$, are consistent with the results of the terrestrial standards suggesting that a small analytical artifact is incorporated in the results. The initial value of $^{41}Ca/^{40}Ca$ is at least 4 times smaller than that of EGG3 according to the detection limit of the instrument based on the measurements of terrestrial standards. The data for HN3-1(c) define a line with a slope $(^{41}Ca/^{40}Ca)_0 = (-4.5 \pm 3.0) \times 10^{-9}$ (2σ) and intercept of $^{41}K/^{39}K = 0.0712 \pm 0.0007$ (2σ) (Table 6). From the Ca-K isochron of 7R-19-1, the values of $(^{41}Ca/^{40}Ca)_0$ and intercept of $^{41}K/^{39}K$ were calculated to be $(-1.7 \pm 1.4) \times 10^{-9}$ (2σ) and 0.0719 ± 0.0004 (2σ), respectively (Table 6).

## DISCUSSION

### Time Scale of Reheating Event between the Formation of $^{16}$O-Rich and $^{16}$O-Poor Melilites in 7R-19-1(a)

The evidence of $^{26}Mg^*$ with the correlation of $^{27}Al/^{24}Mg$ ratios in 7R-19-1 (Table 3; Fig. 4) indicates that short-lived nuclide $^{26}$Al existed at the time of formation of the CAI, having an initial $^{26}Al/^{27}Al$ ratio of $(6.6 \pm 1.3) \times 10^{-5}$. This initial $^{26}Al/^{27}Al$ ratio suggests that the formation environments and stages of 7R-19-1 are similar to other CAIs. Our focus on the Mg isotopic measurement is to estimate the formation time interval between $^{16}$O-rich and $^{16}$O-poor

Table 5. K isotopic data of Allende CAI, EGG3 pyroxene.

| | $^{40}Ca/^{39}K$ (2σ) | $^{41}K/^{39}K$ (2$\sigma_{mean}$) | Mes. Mode |
|---|---|---|---|
| EGG3 pyroxene | | | |
| #01 | (1.06 ± 0.84) × $10^7$ | 0.1437 ± 0.0434 | Circular |
| #02 | (3.00 ± 0.19) × $10^6$ | 0.0821 ± 0.0070 | Circular |
| #03 | (1.04 ± 0.58) × $10^7$ | 0.1410 ± 0.0284 | Circular |
| #04 | (2.39 ± 0.68) × $10^5$ | 0.0664 ± 0.0026 | Circular |
| #05 | (4.81 ± 1.56) × $10^5$ | 0.0733 ± 0.0073 | Circular |
| #06 | (1.94 ± 0.78) × $10^6$ | 0.0582 ± 0.0112 | XY |
| #07 | (3.42 ± 1.36) × $10^7$ | 0.1429 ± 0.0458 | Circular |
| #08 | (5.46 ± 0.87) × $10^7$ | 0.2676 ± 0.1367 | XY |
| #09 | (2.77 ± 1.30) × $10^7$ | 0.1143 ± 0.0606 | Circular |
| EGG3 | Initial $^{40}Ca/^{39}K$ (2σ) | $^{41}K/^{39}K$-intercept (2σ) | |
| | (4.1 ± 2.0) × $10^{-9}$ | 0.0659 ± 0.0042 | |

melilites in 7R-19-1(a) because O isotopic micro-distributions clearly indicate that the $^{16}O$-poor melilite grew after $^{16}O$-rich melilite (Yurimoto et al. 1998; Ito et al. 2004). The single isochron determined by 7R-19-1 indicates that time intervals between the formation of the $^{16}O$-rich and $^{16}O$-poor phases are within the (2σ) analytical errors indicating less than 0.4 Myr. This means that the $^{16}O$-poor melilite crystallized within 0.4 Myr after the $^{16}O$-rich melilite crystallization. We suppose that Mg-Al systematics in $^{16}O$-poor melilite were isotopically homogenized during the melting events.

One possible candidate for quick generation of $^{16}O$-poor reservoir in the early solar system is by CO self-shielding in the X-point region of the nebula (Clayton 2002). Yurimoto and Kuramoto (2004), and Lyons and Young (2005) prefer self-shielding in the molecular cloud and outer region of the protoplanetary disk, respectively. The inner solar nebula was initially $^{16}O$-rich composition and became $^{16}O$-poor with time because of the migration of $^{16}O$-poor water ice into the solar nebula. The $^{16}O$-poor ice water was due to the self-shielding of CO (Clayton 2002; Yurimoto and Kuramoto 2004; Lyons and Young 2005). According to theoretical modeling (Ciesla and Cuzzi 2005), the inner solar system becomes $^{16}O$-depleted within several hundred thousand years since injection and homogenization of $^{26}Al$ in the solar system, which is consistent with our observations.

## Potassium Isotopes in Terrestrial Standards

The $^{41}K/^{39}K$ ratios measured in terrestrial standards with wide range of Ca/K ratios were in good agreement with the terrestrial ratio with the exception of gehlenite (Fig. 3). A line fitted to the all terrestrial standard data has a slope corresponding to $(^{41}Ca/^{40}Ca)_0$ = (–0.4 ± 1.4) × $10^{-9}$ (2σ) (Table 2). Based on the terrestrial standards data, a detection limit of ~$10^{-9}$ can be inferred for the $(^{41}Ca/^{40}Ca)_0$. Generally, melilite in the CAIs shows a wide range of compositions in the gehlenite-åkermanite solid solution system (Grossman 1975). The $^{41}K/^{39}K$ in åkermanite with Ca/K ratio of ~$10^5$ was identical with that of terrestrial value (Fig. 3). The $^{41}K/^{39}K$ in gehlenite with Ca/K ratio of ~3 × $10^6$ overlapped the normal $^{41}K/^{39}K$ composition at 2 limit (Fig. 3). On the other hand, the $^{41}K/^{39}K$ ratio of CAI-Px-2 was in accord with the terrestrial value. As with the $[^{40}Ca^{43}Ca]^{++}/[^{43}Ca]^{+}$ values measured in terrestrial standards and meteoritic phases, those of the synthetic åkermanite, gehlenite, and melilites from HN3-1 and 7R-19-1 were close to each other (Table 4). Therefore, it is not likely that the $[^{40}Ca^{43}Ca]^{++}/[^{43}Ca]^{+}$ values were overestimated for these measurements. The good reproducibility of $^{41}K/^{39}K$ measurements of terrestrial standards further show that our measurement techniques were adequate for meteoritic samples having wide variations of Ca/K ratio.

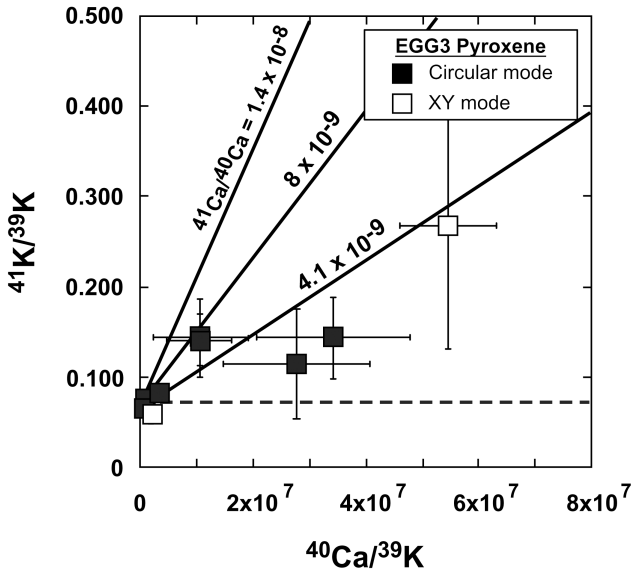


Fig. 5. K isotopic compositions in EGG3 pyroxene from Allende CV3 meteorite. Solid and open squares are measured by circular and XY modes, respectively. Solid lines are 1.4 × $10^{-8}$ (Srinivasan et al. 1996), 8 × $10^{-9}$ (Hutcheon et al. 1984) and 4.1 × $10^{-9}$ (this work). The dashed line represents normal K isotopic composition ($^{41}K/^{39}K$ = 0.072). Error bars for $^{40}Ca/^{39}K$ and $^{41}K/^{39}K$ are ±2σ and ±2$\sigma_m$, respectively.

## Potassium Isotopes in EGG3 Pyroxene

We have measured $^{41}Ca$-$^{41}K$ isotopic systematics in EGG3 pyroxene, whose $^{41}K^*$ from $^{41}Ca$ in situ decay has been published (Hutcheon et al. 1984; Sahijpal et al. 2000), to evaluate $^{41}K^*$ under our measurement conditions using the ims-1270. The Ca/K ratio in EGG3 pyroxene is mostly ~$10^7$ (Table 5). This Ca/K ratio for EGG3 pyroxene was sufficient to detect $^{41}K^*$. Our measured initial $^{41}Ca/^{40}Ca$ value for EGG3 pyroxene (4.1 ± 2.0) × $10^{-9}$, was at least two times smaller than the data of Hutcheon et al. (1984), (8 ± 3) × $10^{-9}$, and that of Sahijpal et al. (2000), (1.17 ± 0.24) × $10^{-8}$ (Fig. 5). The variations of $(^{41}Ca/^{40}Ca)_0$ values of EGG3 pyroxene suggest that the Ca-K system has been disturbed after the CAI

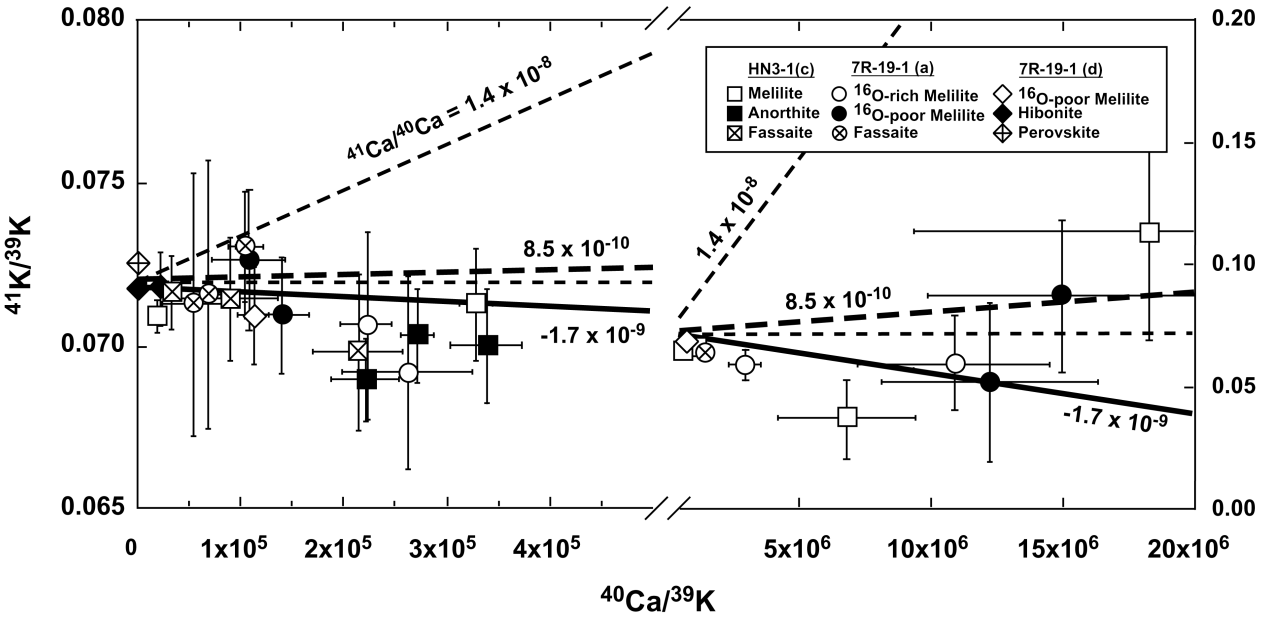


Fig. 6. K isotopic compositions in anorthite, fassaite, hibonite, melilite, and perovskite in 7R-19-1 and HN3-1 from the Allende meteorite. The solid line is the best-fit line for 7R-19-1 indicating $(^{41}Ca/^{40}Ca)_0$ of $-1.7 \times 10^{-9}$. The dashed and long-dashed lines represent the isochrons of $^{41}Ca$-$^{41}K$ isotopic systematics with $(^{41}Ca/^{40}Ca)_0$ of $1.4 \times 10^{-8}$ (Srinivasan et al. 1996), $8.5 \times 10^{-10}$, respectively. The horizontal dashed line represents the reference K isotopic ratio ($^{41}K/^{39}K = 0.072$) (Garner et al. 1975). Error bars for $^{40}Ca/^{39}K$ and $^{41}K/^{39}K$ are $\pm 2\sigma$ and $\pm 2\sigma_m$, respectively.

formation. However, we note the significant lower value for the initial $^{41}K/^{39}K$ of 0.0659 ± 0.0042 (2σ) defined by the EGG3 pyroxene (Table 5). It deviated from the value defined by the terrestrial standards of 0.072 by three standard deviations.

A possible explanation of the small $^{41}K^*$ and the lower $^{41}K/^{39}K$ value may be overestimation of $[^{40}Ca^{42}Ca]^{++}$ interference to $[^{41}K]^+$ for EGG3 pyroxene. According to Table 4, the $[^{40}Ca^{43}Ca]^{++}/[^{43}Ca]^+$ value for EGG3 pyroxene was slightly higher than that of terrestrial standards of CAI-Px-2 and Takashima augite. A possible explanation of smaller $^{41}K^*$ and lower $^{41}K/^{39}K$ in the EGG3 pyroxene have been observed as shown in this study may be due to the overestimation of interference to the mass 41. Despite the uncertainty of the interference correction, the results of EGG3 pyroxene suggest the possible detection of $^{41}K^*$ in CAI minerals having a canonical $(^{41}Ca/^{40}Ca)_0$ value.

**Potassium Isotopes in HN3-1 and 7R-19-1**

The Ca/K ratio in the melilite, fassaite, hibonite, and perovskite from Allende CAIs, HN3-1, and 7R-19-1 vary over a wide range from $10^2$ to $10^7$ (Fig. 6). Because of the expected low value of the initial $^{41}Ca/^{40}Ca$ ratio, ~$10^{-8}$ (e.g., Srinivasan et al. 1994), it is difficult to detect excess $^{41}K$ in any mineral phase with Ca/K < ~$10^5$. However, the Ca/K ratio observed in melilite (Table 6) was sufficiently high for these measurements. The unexpectedly low Ca/K ratio of fassaite, hibonite, and perovskite in HN3-1 and 7R-19-1 may have been due to the primary ion beam overlap onto K-rich phases, such as secondary phases or crystal cracks or due to late stage redistribution of K in crystal after CAI solidification.

According to most previous studies (e.g., Srinivasan et al. 1996), $^{41}K^*$ was correlated with $^{26}Mg^*$ in the same CAIs. CAIs initially had a $(^{41}Ca/^{40}Ca)_0$ value of $1.4 \times 10^{-8}$ together with a canonical $^{26}Al/^{27}Al$ value of $5 \times 10^{-5}$ when formed. We have already discussed how $^{16}$O-poor melilite crystallized within 0.4 Myr after the $^{16}$O-rich melilite crystallization on the basis of the Mg isotopic measurement. If the $^{16}$O-rich melilite in 7R-19-1 initially had a canonical $(^{41}Ca/^{40}Ca)_0$ value of $1.4 \times 10^{-8}$ at its crystallization, the $(^{41}Ca/^{40}Ca)_0$ value of $^{16}$O-poor melilite should have decreased to $8.5 \times 10^{-10}$ within 0.4 Myr (Fig. 6). Since the detection limit of ~$10^{-9}$ can be inferred for the $(^{41}Ca/^{40}Ca)_0$, we should have observed a canonical $(^{41}Ca/^{40}Ca)_0$ value of $1.4 \times 10^{-8}$. However, neither the $^{16}$O-rich nor the $^{16}$O-poor melilites had well resolved $^{41}K^*$ (Fig. 6). Therefore, we conclude that there is no $^{41}K^*$ decay from radioactive $^{41}Ca$ in melilite of 7R-19-1 (Fig. 6). The Ca/K ratios of fassaite, hibonite, and perovskite in 7R-19-1 were not high enough to identify $^{41}K^*$ so the detection of $^{41}K^*$, in these phases cannot be discussed.

According to the O (Yurimoto et al. 1994) and Mg (Koike et al. 1994) isotopic analyses, HN3-1 experienced the multiple heating and/or re-crystallization processes during its formation. Therefore, the lack of $^{41}K^*$ in melilite in HN3-1 may be due to multiple heating processes.

Table 6. K isotopic data of Allende CAIs, HN3-1, and 7R-19-1.[a]

| | $^{40}Ca/^{39}K$ (2σ) | $^{41}K/^{39}K$ (2$\sigma_{mean}$) | | |
|---|---|---|---|---|
| HN3-1(c) | | | | |
| Melilite | | | | |
| HN_Mel#01 | (6.09 ± 0.82) × $10^5$ | 0.0656 ± 0.0029 | | |
| HN_Mel#02 | (3.29 ± 0.16) × $10^5$ | 0.0713 ± 0.0017 | | |
| HN_Mel#03 | (1.09 ± 0.36) × $10^5$ | 0.0726 ± 0.0022 | | |
| HN_Mel#04 | (1.93 ± 0.22) × $10^4$ | 0.0709 ± 0.0005 | | |
| HN_Mel#05 | (1.83 ± 0.89) × $10^7$ | 0.1133 ± 0.0445 | | |
| HN_Mel#06 | (9.97 ± 4.11) × $10^5$ | 0.0644 ± 0.0054 | | |
| HN_Mel#07 | (6.84 ± 2.62) × $10^6$ | 0.0373 ± 0.0161 | | |
| Anorthite | | | | |
| HN_An#01 | (2.22 ± 0.32) × $10^5$ | 0.0690 ± 0.0012 | | |
| HN_An#02 | (3.39 ± 0.35) × $10^5$ | 0.0700 ± 0.0018 | | |
| HN_An#03 | (2.72 ± 0.16) × $10^5$ | 0.0704 ± 0.0014 | | |
| Fassaite | | | | |
| HN_Fas#01 | (2.15 ± 0.44) × $10^5$ | 0.0698 ± 0.0024 | | |
| HN_Fas#02 | (9.03 ± 4.79) × $10^4$ | 0.0715 ± 0.0019 | | |
| HN_Fas#03 | (3.36 ± 0.52) × $10^4$ | 0.0717 ± 0.0011 | | |
| 7R-19-1(a) | | | O isotope[b] | Al-Mg No.[c] |
| Melilite | | | | |
| a_Mel#01 | (1.23 ± 0.41) × $10^7$ | 0.0520 ± 0.0320 | $^{16}$O-poor | Ma#02 |
| a_Mel#02 | (2.63 ± 0.63) × $10^5$ | 0.0692 ± 0.0030 | $^{16}$O-rich | Ma#03 |
| a_Mel#03 | (2.23 ± 0.25) × $10^5$ | 0.0707 ± 0.0029 | $^{16}$O-rich | |
| a_Mel#04 | (1.04 ± 0.08) × $10^5$ | 0.0737 ± 0.0017 | $^{16}$O-poor | Ma#05 |
| a_Mel#05 | (1.10 ± 0.37) × $10^7$ | 0.0599 ± 0.0194 | $^{16}$O-rich | |
| a_Mel#06 | (1.50 ± 0.52) × $10^7$ | 0.0873 ± 0.0310 | $^{16}$O-poor | Ma#02 |
| a_Mel#07 | (1.41 ± 0.27) × $10^5$ | 0.0710 ± 0.0018 | $^{16}$O-poor | Ma#05 |
| a_Mel#08 | (2.94 ± 0.58) × $10^6$ | 0.0593 ± 0.0065 | $^{16}$O-rich | |
| Fassaite | | | | |
| a_Fas#01 | (5.52 ± 2.91) × $10^4$ | 0.0713 ± 0.0040[c] | | |
| a_Fas#02 | (6.93 ± 1.31) × $10^4$ | 0.0716 ± 0.0041[c] | | |
| a_Fas#03 | (1.06 ± 0.17) × $10^5$ | 0.0731 ± 0.0022[c] | | Fa#01 |
| a_Fas#04 | (1.42 ± 0.27) × $10^6$ | 0.0657 ± 0.0060[c] | | |
| 7R-19-1(d) | | | | |
| Melilite | | | | |
| d_Mel#01 | (8.02 ± 1.15) × $10^5$ | 0.0708 ± 0.0021 | $^{16}$O-poor | Md#03 |
| d_Mel#02 | (1.13 ± 0.15) × $10^5$ | 0.0710 ± 0.0015 | $^{16}$O-poor | |
| Hibonite | | | | |
| d_Hib#01 | (1.20 ± 0.05) × $10^3$ | 0.0717 ± 0.0003 | $^{16}$O-rich | Hd#01,02 |
| d_Hib#02 | (2.31 ± 0.26) × $10^4$ | 0.0718 ± 0.0011 | $^{16}$O-rich | |
| Perovskite | | | | |
| d_Pev#01 | (3.10 ± 1.44) × $10^2$ | 0.0725 ± 0.0006 | $^{16}$O-poor | |
| | Initial $^{40}Ca/^{39}K$ (2σ) | $^{41}K/^{39}K$-intercept (2σ) | | |
| HN3-1 | (–4.5 ± 3.0) × $10^{-9}$ | 0.0712 ± 0.0007 | | |
| 7R-19-1 | (–1.7 ± 1.4) × $10^{-9}$ | 0.0719 ± 0.0004 | | |

[a]All data were obtained by circular mode.
[b]O isotopic characteristics was determined by Yurimoto et al. (1998) and Ito et al. (2004).
[c]Corresponding to the measured points of Mg isotopes in Table 3.

A couple of suggestions have been made to explain the nondetection of the short-lived nuclide $^{41}$Ca in the 7R-19-1. One possibility is that $^{41}$Ca was not present in 7R-19-1 at the time of its crystallization. Srinivasan and Bischoff (2001) made a similar suggestion on the basis of the lack of correlation between $^{26}Mg^*$ and $^{41}K^*$ in the CAI022/1 from the CH chondrite Acfer 182. Alternatively, $^{41}$Ca may have been present at the time of crystallization of 7R-19-1, but the $^{41}K^*$ was erased through the thermal history after at least a half million years of CAI formation.

### Loss/Redistribution of Potassium in Melilite

Refractory minerals of spinel, fassaite, and melilite in 7R-19-1(a) showed large negative anomalies of $\Delta^{17}O$ in the following order: spinel (−21‰) > $^{16}$O-rich melilite (−18‰) > fassaite (−15 to +1 ‰) > $^{16}$O-poor melilite (−8 to +2‰) (Yurimoto et al. 1998; Ito et al. 2004). A sharp zoning pattern within a single crystal of melilite in 7R-19-1(a) was discovered by Yurimoto et al. (1998), who invoked a remelting event to explain the isotopic exchange pattern.

Yurimoto et al. (1998) have measured the rare earth element (REE) patterns in fassaite and $^{16}$O-rich and $^{16}$O-poor melilites in 7R-19-1(a). REE patterns in the $^{16}$O-rich melilite (Mel$^*$) of the 7R-19-1(a) were fractionated by an igneous process as the CAI crystallized from an original melt. The Mel$^*$ had a light REE enrichment and slightly negative anomaly of Eu. The $^{16}$O-poor melilite (Mel) had an identical igneous derived REE pattern except for a constant enrichment factor for all but Eu and Yb. A complementary REE pattern to $^{16}$O-rich melilite was found in fassaite. A very brief heating event was suggested to have melted and partially vaporized the Mel$^*$ of CAI making Mel with a uniform REE enrichment relative to the Mel. The most volatile elements of Eu and Yb were apparently lost during the vaporization. The vaporization during heating/melting was supported by the REE patterns of Mel$^*$, Mel, and fassaite in 7R-19-1(a).

As a result of O isotope distributions and REE patterns of melilite and fassaite in 7R-19-1(a), the K vaporization from the melt might also have occurred during the heating/melting processes. In 7R-19-1(a), $^{16}$O-poor melilite tends to be depleted in K relative to the adjacent $^{16}$O-rich melilite (Table 6) because the average $^{40}$Ca/$^{39}$K ratio in $^{16}$O-poor melilite is more than that of $^{16}$O-rich melilite. The depletion of K suggests that the evaporation has occurred between the melting of $^{16}$O-rich melilite and crystallization of $^{16}$O-poor melilite. Humayun and Clayton (1995) reported that $^{41}$K/$^{39}$K was effectively uniform in the residual condensed phase because the diffusivity of K in evaporating material was sufficiently rapid. Therefore, $^{41}$K/$^{39}$K ratio may not be changed during evaporation process if K was experienced lost and/or redistribution.

According to a previous study (Ito and Ganguly 2004), the K diffusivity in melilite was one half of an order of magnitude smaller than the O diffusivity in melilite (Yurimoto et al. 1989). Oxygen isotopic distribution in melilite was not largely modified after the melilite crystallization (Yurimoto et al. 1998; Ito et al. 2004). Therefore, erasing of $^{41}$K$^*$ in the melilite crystals cannot be supported by the diffusion process.

## CONCLUSIONS

The $^{26}$Al-$^{26}$Mg and $^{41}$Ca-$^{41}$K isotopic systematics in CAIs 7R-19-1 and HN3-1 and EGG3 pyroxene grains from Allende CV3 meteorite were measured using secondary ion mass spectrometry. Resulting from the $^{26}$Al-$^{26}$Mg systematics for $^{16}$O-rich and $^{16}$O-poor melilite grains in 7R-19-1, the time interval between the individual melting stages occurred within 0.4 Myr. We cannot detect radiogenic $^{41}$K$^*$ in melilite, fassaite, perovskite, or anorthite in CAIs 7R-19-1 and HN3-1, suggesting that $^{41}$Ca was absent in 7R-19-1 and HN3-1 at the initial stage of crystallization. The value of $(^{41}Ca/^{40}Ca)_0$ in EGG3 pyroxene was $(4.1 \pm 2.0) \times 10^{-9}$ (2σ), which is about two times smaller than the previous results (Hutcheon et al. 1984; Sahijipal et al. 2000).

*Acknowledgments*–Comments and suggestions by Dr. A. Krot, Dr. J. N. Goswami, Dr. I. D. Hutcheon, Dr. S. Sahijipal, and associate editors Dr. E. K. Zinner and Dr. I. Lyon resulted in significant improvement to the paper and are gratefully acknowledged. We are grateful to Dr. J. N. Goswami for providing us with an EGG3 pyroxene sample of Allende meteorite and CAI-Px-2 standard for this study and for discussion and Dr. M. Morioka for his help in synthesizing åkermanite and gehlenite crystals at the Radio Isotope Centre, University of Tokyo. We thank Dr. S. Messenger of NASA, JSC for improvement of English and discussion.

*Editorial Handling*—Dr. Ian Lyon

## REFERENCES

Bizzarro M., Baker J. A., and Haack H. 2004. Mg isotope evidence for contemporaneous formation of chondrules and refractory inclusions. *Nature* 431:275–278.

Clayton R. N. 2002. Photochemical self-shielding in the solar nebula (abstract #1326) 33rd Lunar and Planetary Science Conference. CD-ROM.

De Chambost E., Schuhmacher M., Lovestam G., and Claesson S. 1997. Achieving high transmission with the Cameca IMS 1270. In *Secondary ion mass spectrometry*, edited by Benninghoven A., Hagenhoff B. B., and Werner H. W. New York: John Wiley & Sons. pp. 1003–1006.

Garner E. L., Murphy T. J., Gramlich J. W., Paulsen P. J., and Barnes I. L. 1975. Absolute isotopic abundance ratio and the atomic weight of a reference sample of potassium. *Journal of Research of the National Bureau of Standards* 79A:713–725.

Grossman L. 1975. Petrography and mineral chemistry of Ca-rich inclusions in the Allende meteorite. *Geochimica et Cosmochimica Acta* 39:439–454.

Humayun M. and Clayton R. N. 1995. Potassium isotope geochemistry: Genetic implications of volatile element depletion. *Geochimica et Cosmochimica Acta* 59:2131–2148.

Hutcheon I. E., Armstrong J. T., and Wasserberg G. J. 1984. Excess $^{41}$K in Allende CAI: A hint re-examined (abstract). *Meteoritics* 19:243.

Ireland T. R., Zinner E., Sahijpal S., and McKeegan K. D. 1999. Confirmation of excess $^{41}$K from $^{41}$Ca decay in refractory inclusion (abstract). *Meteoritics & Planetary Science* 34:A57.

Ito M. 1999. Oxygen isotopic microanalysis by SIMS: A study of the formation process and thermal history of the Allende meteorite in the early solar system. Ph.D. thesis, Gakushun University, Tokyo, Japan.

Ito M. and Ganguly J. 2004. Potassium diffusion in melilite:

Experimental studies and constraints on the thermal history and size of planetesimals hosting CAIs. *Meteoritics & Planetary Science* 39:1911–1920.

Ito M., Yurimoto H., and Nagasawa H. 2004. Oxygen isotopic SIMS analysis in Allende CAI: Details of the very early thermal history of the solar system. *Geochimica et Cosmochimica Acta* 68:2905–2923.

Koike O., Yurimoto H., and Nagasawa H. 1994. Al-Mg isotopic and REE clues to the formation to a type B1 CAI of Allende meteorite (abstract). 25th Lunar and Planetary Science Conference. pp. 725–726.

Lyons J. R. and Young E. D. 2005. CO self-shielding as the origin of oxygen isotope anomalies in the early solar nebula. *Nature* 435: 317–320.

MacPherson G. J., Davis A. M., and Zinner E. K. 1995. The distribution of aluminum-26 in the early solar system—A reappraisal. *Meteoritics* 30:365–377.

Maruyama S. and Yurimoto H. 2003. Relationship among O, Mg isotopes and the petrography of two spinel-bearing compound chondrules. *Geochimica et Cosmochimica Acta* 67:3943–3957.

Mayeda T. K., Clayton R. N., and Nagasawa H. 1986. Oxygen isotope variations within Allende refractory inclusions (abstract). 17th Lunar and Planetary Science Conference. pp. 526–527.

Meeker G. P., Wasserburg G. J., and Armstrong J. T. 1983. Replacement textures in CAI and implications regarding planetary metamorphism. *Geochimica et Cosmochimica Acta* 47: 707–721.

Nagahara H., Nagasawa H., Nakamura N., and Matsui T. 1987. HN3-1 (type B-1 CAI) formed from isotopically and chemically heterogeneous interstellar minerals and condensates of the solar system by incompatible melting (abstract). 18th Lunar and Planetary Science Conference. pp. 694–695.

Sahijpal S., Goswami J. N., Davis A. M., Grossman L., and Lewis R. S. 1998. A stellar origin for the short-lived nuclides in the early solar system. *Nature* 391:559–561.

Sahijpal S., Goswami J. N., and Davis A. M. 2000. K, Mg, Ti, and Ca isotopic compositions and refractory trace element abundances in hibonite from CM and CV meteorites: Implications for early solar system processes. *Geochimica et Cosmochimica Acta* 64: 1989–2005.

Srinivasan G., Ulyanov A. A., and Goswami J. N. 1994. $^{41}$Ca in the early solar system. *The Astrophysical Journal* 431:L67–70

Srinivasan G., Sahijpal S., Ulyanov A. A., and Goswami J. N. 1996. Ion microprobe studies of Efremovka CAIs: II. Potassium isotope composition and $^{41}$Ca in the early solar system. *Geochimica et Cosmochimica Acta* 60:1823–1835.

Srinivasan G. and Bischoff A. 2001. Ca-K and Al-Mg studies of CAIs from CH and CR chondrite (abstract). *Meteoritics & Planetary Science* 36:A196.

Ushikubo T., Hiyagon H., and Sugiura N. 2000. A FUN-like hibonite inclusion in Kainsaz CO3 chondrite with large $^{41}$K and $^{26}$Mg excesses at the level of normal CAIs (abstract #1561). 31st Lunar and Planetary Science Conference. CD-ROM.

Yurimoto H. and Kuramoto K. 2004. Molecular cloud origin for the oxygen isotope heterogeneity in the solar system. *Science* 305: 1763–1766.

Yurimoto H., Morioka M., and Nagasawa H. 1989. Diffusion in single crystals of melilite: I. Oxygen. *Geochimica et Cosmochimica Acta* 53:2387–2394.

Yurimoto H., Nagasawa H., Mori Y., and Matsubaya O. 1994. Micro-distribution of oxygen isotopes in a refractory inclusion from the Allende meteorite. *Earth and Planetary Science Letters* 128:47–53.

Yurimoto H., Ito M., and Nagasawa H. 1998. Oxygen isotope exchange between refractory inclusion in Allende and solar nebula gas. *Science* 282:1874–1877.